MICROSTRUCTURAL INVESTIGATION OF PORTLAND-LIMESTONE CEMENT CONCRETE WITH POZZOLANIC MATERIALS AFTER LONG-TERM EXPOSURE TO SULFATE ENVIRONMENT

K. Sotiriadis[1,*], P. Mácová[1], A. Mazur[2], A. Viani[1], S. Tsivilis[3]
[1]Institute of Theoretical and Applied Mechanics of the Czech Academy of Sciences, Prague, Czechia
[2]Center for Magnetic Resonance, St. Petersburg State University, Petergof, St. Petersburg, Russia
[2]School of Chemical Engineering, National Technical University of Athens, Athens, Greece
(*sotiriadis@itam.cas.cz)

ABSTRACT
In the present study, identification and quantification of the phases present in samples obtained from the surface of deteriorated Portland-limestone cement concrete specimens, incorporating pozzolanic materials, was performed, after long-term exposure to sulfate solution at 5 °C, employing a combination of analytical techniques. The results indicated that thaumasite was more abundant in concrete without pozzolanic addition. Destabilization of thaumasite, occurring in concrete with natural pozzolana, was accompanied by increased gypsum and amorphous content. Metakaolin most effectively prevented C–S–H degradation. Pozzolanic materials contributed in increased mean chain length of C–(A–)S–H structures. Al substitution for Si in silicate chains was more pronounced in concrete with pozzolans.

INTRODUCTION
The global trend towards the production of building materials with low environmental impact, concerning reduction of CO_2 emissions, decrease of production energy needs, rationalization of raw materials usage, and exploitation of industrial by-products, has led to the employment of special types of cement and natural or artificial pozzolanic materials in concrete production.
Portland-limestone cements belong to one of these types, identified in the European standard EN 197-1 [1], with properties competitive to those of ordinary Portland cement [2]. However, limestone content increases the risk for chemical attack on concrete made from these cements, especially when in contact with groundwater containing SO_4^{2-} at low temperature (5°C). In such case, sulfate and carbonate ions react with the calcium silicate hydrate (C–S–H) phase of the hardened cement paste, which provide most of concrete's mechanical strength [3]. As a result, C–S–H is consumed, while thaumasite ($CaSiO_3 \cdot CaCO_3 \cdot CaSO_4 \cdot 15H_2O$) forms, leading to concrete degradation [4]. Concrete durability can be improved by introducing pozzolanic materials in the mixture, as partial replacement of Portland-limestone cement [5], resulting in both physical and chemical changes [6, 7]. The interdependence between the processes of thaumasite formation and C–S–H phase degradation is of importance when dealing with concrete exposed to conditions promoting thaumasite sulfate attack (TSA). Correlation of the amounts of the two phases may indicate the degree of concrete deterioration. The technique of election for the quantification of the phases in deteriorated concrete samples is X-ray powder diffraction (XRPD) combined with the Rietveld method. Although crystalline phases can be easily distinguished with XRPD, the amorphous fraction of the sample is detected as a single phase, thus, amorphous products and the poorly crystalline C–S–H phase [8] cannot be distinguished.
Solid state nuclear magnetic resonance (ssNMR) spectroscopy has also been considered for studying such systems, because it allows for identifying and quantifying both crystalline and amorphous phases, based on its selectivity of specific nuclei [9]. The technique suffers sometimes from pure resolution and long counting times, depending on the natural abundance of nuclei. Previous studies demonstrated the reliability of ssNMR for the qualitative and quantitative determination of thaumasite in cementitious materials affected by sulfate attack [10, 11].

AIM AND METHODOLOGY

The objective of the study is to investigate the phase composition in samples obtained from the deteriorated surface of Portland-limestone cement concretes, incorporating pozzolanic materials, after long-term exposure to sulfate solution at 5 °C. A combination of analytical techniques (XRPD, Fourier-transform infrared (FTIR) spectroscopy, ssNMR) were employed to characterize and quantify both crystalline and amorphous fraction of the samples. Getting new insights into long-term deterioration process and relating it to concrete composition is the novelty of the approach.

EXPERIMENTAL

Portland-limestone cement with 15% w/w limestone content was produced in laboratory, by intergrinding industrial clinker, limestone of high calcite content (97.5%) and gypsum, in a pilot plant ball mill of 5 kg capacity. The 28-day compressive strength and specific surface (Blaine method) achieved were 41.3 MPa and 3980 cm^2/g, respectively. Binders were prepared by replacing part of the cement produced (LC) with 30% natural pozzolana (LPC), 50% blastfurnace slag (LSC), and 10% metakaolin (LMC). The mineralogical composition of the materials used is given in Table 1. Concretes were produced using binder content of 350 kg/m^3, water-to-binder ratio of 0.52 and calcareous aggregates (16 mm maximum size). Cubic specimens were casted (100×100×100 mm), left in the molds for 24 h, then water-cured for 6 days at ambient conditions, and finally air-cured for 21 days in laboratory conditions. Immersion of the specimens in $MgSO_4$ solution (20 g/L SO_4^{2-} content) and storage at 5 °C for 10 years followed the initial curing period. The specimens remained at ambient temperature for an additional year, until the solution was gradually evaporated.

Table 1. *Chemical composition (% w/w) of clinker and pozzolanic materials.*

Compound	Clinker (K)	Limestone (L)	Natural pozzolana (P)	Blastfurnace slag (S)	Metakaolin (M)
SiO_2	21.92	0.57	65.30	39.49	54.41
Al_2O_3	5.68	0.33	13.94	10.14	43.94
CaO	63.35	54.60	4.01	39.97	0.37
Other oxides	8.13	1.89	10.71	8.43	0.66
LOI	0.91	42.76	5.32	0.16	—
fCaO	1.15	—	—	—	—

The samples used for the analyses were milled, prior to testing, to achieve particle size ≤63 μm.
XRPD analysis was performed using a Bruker D8 Advance diffractometer; data were collected in the angular range 4–82° 2ϑ, at 40 kV and 40 mA, with Cu Ka radiation (λ = 1.5418 Å), virtual step scan of 0.0102° 2ϑ, counting time of 0.4 s/step, and sample's rotating speed of 15 rpm. Spiking each sample with 10 wt.% of internal standard α-Al_2O_3 (NIST SRM 676a) allowed for quantitative phase analysis (QPA); Rietveld refinements were accomplished with TOPAS 4.2 software (Bruker ASX).
FTIR spectra were acquired at ambient temperature at 4 cm^{-1} resolution in the range 4000–550 cm^{-1}, using an external module iZ10 of Nicolet iN10 spectrometer (Thermo Scientific), equipped with DTGS detector, KBr beamsplitter and smart ATR accessory with diamond crystal.
One-pulse ^{29}Si NMR spectra were obtained at 25 °C using a Bruker Avance III 400 WB NMR spectrometer. For magnetic field of 9.4 T, the corresponding Larmor frequency for ^{29}Si nuclei is 79.5 MHz. Samples were loaded into a ZrO_2 rotor (4 mm in diameter) and spun at 12.5 kHz under MAS (magic angle spinning) regime. 10000 scans were recorded with 4 μs pulse length and 5 s relaxation delay. Component deconvolution was performed with PeakFit 4.12 software (Systat Software, Inc.).

RESULTS AND DISCUSSION

The results of QPA are presented in Table 2. The agreement factor for the refinements (R_{wp}) was in the range 6.5–7.0%. Calcite is the most abundant crystalline phase detected in all samples, with

weight fraction ranging from 36.1 to 53.6 wt.%. Gypsum and thaumasite were identified as secondary phases. Small amounts of aragonite and traces of brucite and quartz were also found.

Table 2. *QPA (wt.%) as determined by Rietveld refinement of the XRPD patterns.*

Phase	LC	LPC	LSC	LMC
Thaumasite	12.8	4.8	4.2	3.1
Gypsum	8.3	20.6	8.4	7.5
Calcite	45.1	36.1	51.7	53.6
Aragonite	4.8	2.3	3.9	5.3
Brucite	0.2	–	0.5	0.5
Quartz	0.3	0.5	0.3	0.3
Amorphous	28.5	35.7	31.0	29.7

The amount of thaumasite is significantly higher in sample LC than in samples containing pozzolanic materials, and also higher than that of gypsum, contrary to what observed in the samples LPC, LSC and LMC. This indicates the contribution of pozzolanic materials in decreasing thaumasite formation. The very high amount of gypsum and amorphous fraction in sample LPC, compared to the other samples, implies that the degradation process led to the destabilization of thaumasite as a result of a drop in system's pH, occurred due to C–S–H decalcification, the effect of Mg^{2+} on C–S–H, or carbonation [12, 13]. The presence of brucite is indicative of decreased pH in the system [14]. Reduction of pH towards 7 destabilizes thaumasite leading to the precipitation of popcorn calcite, assumed as the final stage of TSA [12], and to gypsum and silica-rich gel (or amorphous SiO_2) formation [15]:

$$Thaumasite + H_2O \rightarrow CaCO_3 + Ca^{2+} + SO_4^{2-} \pm CaSO_4 \cdot 2H_2O + (Ca-)Si - H_2O \quad (1)$$

Aragonite has been detected in TSA-affected cementitious materials in the presence of magnesium ions in the corrosive environment and its formation was facilitated at 20 °C [16]. This is in agreement with the conditions applied at the final stage of the present study. Quartz identified could be considered as a contamination of the raw materials used.

The ATR-FTIR spectra collected are illustrated in Figure 1; they indicate the presence of gypsum, calcium carbonates (calcite and aragonite), thaumasite and brucite, confirming the XRPD results.

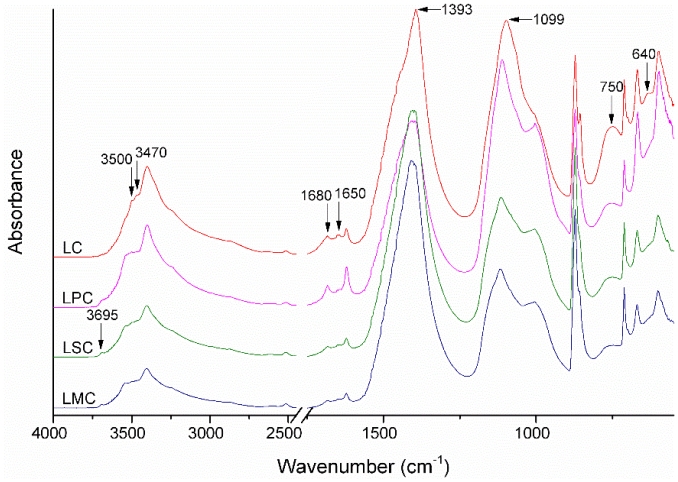

Figure 1. *ATR-FTIR spectra collected for all samples; main peaks are indicated.*

The weak peak at 3695 cm^{-1}, with highest intensity in samples LSC and LMC, is attributed to O–H stretch vibration in brucite [17]. Characteristic bands of thaumasite appear in all spectra and, in agreement with Sholtzová et al. [18], the attribution is as follows. The peaks at 3500 and 3470 cm^{-1} are assigned to O–H asymmetric stretching modes; the peaks at 1680 and 1650 cm^{-1} indicate O–H bending vibrations of H_2O, splitting due to non-equivalent water molecules in the crystal structure.

Gypsum also contributes the band at 1680 cm^{-1}. The peak at 750 cm^{-1} is due to Si–O symmetric stretching vibration of $Si(OH)_6^{2-}$; the peak at 640 cm^{-1} originates from Si–O symmetric stretching modes, O–C–O and O–S–O bending modes. The strong peak of thaumasite at 1395 cm^{-1} (C–O asymmetric stretching vibration of carbonate groups) overlaps with the same vibration mode of calcium carbonate. Higher thaumasite content results in shifting the maximum of this peak towards lower wavenumber (from 1420 cm^{-1} in LMC to 1393 cm^{-1} in sample LC). Another strong peak of thaumasite at 1099 cm^{-1} (S–O asymmetric stretching modes of SO_4^{2-}) overlaps with the same vibration mode in gypsum. The higher amount of thaumasite shifts the maximum of this peak to lower wavenumber (from ~1115 cm^{-1} in LMC to 1099 cm^{-1} in sample LC). Vibration bands of C–S–H and C–A–S–H in range 1100–900 cm^{-1} are in strong overlap with other phases, complicating the assignment. More information about C–S–H phase is provided from the results of ssNMR.

Figure 2 depicts the one-pulse ^{29}Si MAS NMR spectra obtained. Each spectrum has been deconvoluted and the identified components are indicated. In all spectra, two distinct signals are clearly observed. A sharp resonance at approx. –197.5 ppm is characteristic of silicon in octahedral SiO_6 coordination [19], corresponding to thaumasite which is the only mineral in cementitious systems with silicon in octahedral environment [10]. The intensity in LC is the higher, confirming XRPD results.

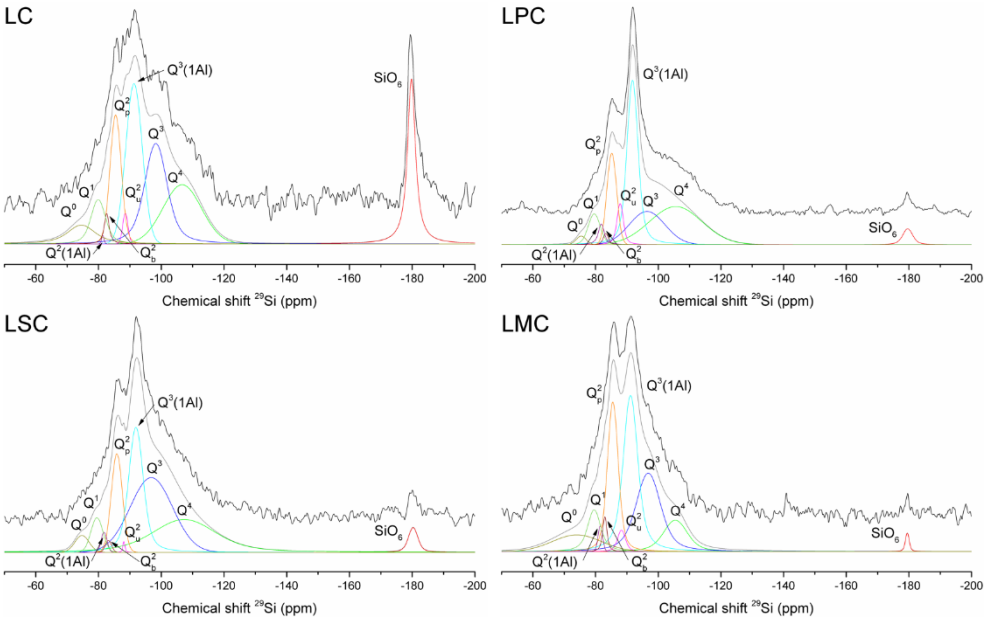

Figure 2. *^{29}Si MAS NMR spectra acquired from each sample. Black curves: experimental spectra; Coloured curves: deconvoluted spectra; Grey curves: sum of the components.*

The second is a broader signal, including two sharper resonances, emerged at isotropic chemical shift values (δ_{iso}) between –120 ppm and –60 ppm, indicating silicon in tetrahedral SiO_4 coordination [20]. Deconvolution allowed for the distinction of nine non-equivalent silicon environments in this range, which partially overlap. This procedure was performed keeping fixed the position of each component, according to Meyers et al [21]. Q^n notation has been used to specify the bands, where Q stands for a SiO_4^{4-} unit and n is the degree of connectivity, corresponding to the number of oxygen-linked SiO_4^{4-} units [20]. The attribution of each resonance is as follows [21-24]: –75 ppm (anhydrous silicate species, Q^0); –80 ppm (end groups in C–S–H, Q^1); –82 ppm (silicate units interconnected through AlO_4 tetrahedron in C–S–H, $Q^2(1Al)$); –83 ppm (bridging positions in C–S–H, Q_b^2); –85 ppm (pairing positions in C–S–H, Q_p^2); –89 ppm (bridging positions in C–S–H bound to H^+, Q_u^2); –92 ppm (silicate units in branching positions of chains incorporating AlO_4 tetrahedron, $Q^3(1Al)$); –96 ppm (branching sites of silicate chains, Q^3); and –106 ppm (condensed silicate groups, Q^4).

Since the technique is quantitative, the integrated area below each deconvoluted signal is proportional to the amount of nuclei in each component. Results are summarized in Table 3. Besides

Q^1 and Q^2 species, which are typical for C–S–H, Q^3 and Q^4 also appear, which are not normally present in C–S–H [24]. Such species indicate a cross-linked silicate network with a layered structure similar to clays, found also in M–S–H [25, 26]. The latter is a product of attack of Mg^{2+} on C–S–H, which degrades its binding properties. In all samples, the amounts of Q^3 and Q^4 species are significantly higher than those of Q^1 and Q^2 species, denoting deterioration of C–S–H phase. Assuming the ratio $\frac{Q^1 + Q^2}{Q^3 + Q^4}$ as an indicator of C–S–H damage, we observe that metakaolin was the most effective pozzolanic material in preventing C–S–H degradation in Portland-limestone cement concrete, in contrast to blastfurnace slag, which was the least effective one. LPC composition shows similar results with the LC; the large amounts of Q^3 and Q^4 components in LPC are contributed also by thaumasite decomposition (Equation 1). The presence of Q^2(1Al) and Q^3(1Al) species implies the incorporation of Al in silicate chains.

Table 3. *Component deconvolution (area %) of the ^{29}Si MAS NMR spectra collected.*

Component	LC	LPC	LSC	LMC
SiO_6	14.7	2.5	2.8	0.8
Q^0	5.2	1.1	2.4	8.2
Q^1	6.0	5.2	4.2	7.0
Q^2(1Al)	0.2	2.2	1.2	1.2
Q^2_b	1.6	0.9	0.7	2.0
Q^2_p	11.8	12.0	11.0	18.7
Q^2_u	1.3	4.3	0.3	2.1
Q^3(1Al)	20.8	28.9	21.5	28.2
Q^3	20.7	15.9	31.9	22.9
Q^4	17.9	26.9	23.9	8.9

In Table 4, the values of mean chain length and average AlO_4/SiO_4 tetrahedra molar ratio in non-cross-linked (nc) and cross-linked (c) C–(A–)S–H structures are presented, calculated from the relevant equations reported by Myers et al. [22].

Table 4. *Mean chain length (MCL) and average Al/Si tetrahedra molar ratio of no cross-linked (nc) and cross-linked (c) of aluminosilicate chains.*

Composition	$MCL_{(nc)}$	$Al/Si_{(nc)}$	$MCL_{(c)}$	$Al/Si_{(c)}$
LC	7.01	0.004	55.7	0.33
LPC	9.89	0.046	75.7	0.42
LSC	8.64	0.034	88.6	0.30
LMC	9.03	0.019	63.2	0.34

The employment of pozzolanic materials in concrete mixtures resulted in longer mean chain length in both C–(A–)S–H structures, compared to pure Portland-limestone cement concrete. This observation, along with the higher content of thaumasite in LC composition, denotes that the process moved mostly towards C–S–H decomposition. Non-cross-linked chains were shorter in LSC sample than in LPC and LMC, contrary to cross-linked chains, denoting greater polymerization when blastfurnace slag was used.

The incorporation of Al in non-cross-linked silicate chains is larger in compositions containing pozzolans, which is most likely related to their higher content in Al_2O_3. According to previous study, lower Ca/Si content in cement causes an increased Al incorporation into C–S–H [27], which is the case here. Notably, although the highest aluminum content is that of LMC composition, it seems that it was not incorporated in C–S–H in such extent as in the case of LPC and LSC compositions. Regarding

cross-linked chains, i.e. chains produced from deteriorated C–S–H, the $Al/Si_{(c)}$ values are quite similar among all samples and always higher than the $Al/Si_{(nc)}$ ones, indicating that most of the chains containing Al were already not part of C–S–H fraction. Deterioration of C–S–H, related mainly to depletion of Ca and decrease of Ca/Si ratio in this phase, allowed for greater Al in silicate chains.

CONCLUSIONS

The larger amount of thaumasite was detected in Portland-limestone cement concrete without any pozzolanic addition. In concrete composition with natural pozzolana, destabilization of thaumasite occurred, indicated by increased gypsum and amorphous content. Metakaolin was the most effective pozzolanic addition to inhibit C–S–H degradation contrary to blastfurnace slag. Pozzolanic materials contributed in increased mean chain length of both non-cross-linked and cross-linked C–(A–)S–H structures. Al substitution for Si in silicate chains was more pronounced in concrete incorporating pozzolanic materials.

ACKNOWLEDGEMENTS

This study was performed in the frame of the research project “Experimental quantification and modelling of deterioration in Portland-limestone cement pastes affected by thaumasite sulfate attack”, funded by the Czech Science Foundation (project number: 18-26056Y).

REFERENCES

[1] CEN (European Committee for Standardization). EN 197-1:2011, EN/TC 51/WG-6.
[2] S. Tsivilis, G. Batis, E. Chaniotakis, G. Grigoriadis, D. Theodossis. *Cem. Concr. Res.* 30(10) (2000) 1679–83.
[3] E Taujelo Rodríguez, K. Garbev, D. Merz, L. Black, I.G. Richardson. *Cem. Concr. Res.* 93 (2017) 45–56.
[4] N.J. Crammond. *Cem. Concr. Compos.* 25(8) (2003) 809–18.
[5] K. Sotiriadis, E. Nikolopoulou, S. Tsivilis, A. Pavlou, E. Chaniotakis, R.N. Swamy. *Constr. Build. Mater.* 43 (2013) 156–64.
[6] S.U. Khan, M.F. Nuruddin, T. Ayub, N. Shafiq. *Sci. World J.* (2014) 986567.
[7] F. Bellmann, J. Stark. *Cem. Concr. Res.* 37(8) (2007) 1215–22.
[8] I.G. Richardson. *Cem. Concr. Res.* 38(2) (2008) 137–58.
[9] J. Skibsted, C. Hall. *Cem. Concr. Res.* 38(2) (2008) 205–25.
[10] J. Skibsted, L. Hjorth, H.J. Jakobsen. *Adv. Cem. Res.* 7(26) (1995) 69–83.
[11] J. Skibsted, S. Rasmussen, D. Hertfort, H.J Jakobsen. *Cem. Concr. Compos*. 25(8) (2003) 823–9.
[12] N. Crammond. *Cem. Concr. Compos.* 25(8) (2003) 809–18.
[13] Z. Liu, D. Deng, G. De Schutter, Z. Yu. *Cem. Concr. Compos.* 35(1) (2010) 34–42.
[14] S.A. Hartshorn, J.H. Sharp, R.N. Swamy. *Cem. Concr. Res.* 29(8) (1999) 1331–40.
[15] P. Hagelia, R.G. Sibbick. *Mater. Charact.* 60(7) (2009) 686–99.
[16] S.A. Hartshorn, J.H. Sharp, R.N. Swamy. *Cem. Concr. Compos.* 24(3–4) (2002) 351–9.
[17] T.L. Hughes, C.M. Methven, T.G.J. Jones, S.E. Pelham, P. Fletcher, C. Hall. *Adv. Cem. Based Mater.* 2(3) (1995) 91–104.
[18] E. Scholtzová, L. Kucková, J. Kožíšek, H. Pálková, D. Tunega. *Cem. Concr. Res.* 59 (2014) 66–72.
[19] A.R. Grimmer, F. von Lampe, M. Mägi. *Chem. Phys, Lett.* 132(6) (1986) 549–53.
[20] G. Engelhardt. Encyclopedia of Magnetic Resonance (Eds. R.K. Harris and R. Wasylishen), John Wiley & Sons, Ltd., Chichester, UK.
[21] R.J. Myers, E. L’Hôpital, J.L Provis, B. Lothenbach. *Cem. Concr. Res.* 68 (2015) 83–93.
[22] D. Gastaldi, G. Paul, L. Marchese, S. Irico, E. Boccaleri, S. Mutke, L. Buzzi, F. Canonico. *Cem. Concr. Res.* 90 (2016) 162–73.
[23] E. L’Hôpital, B. Lothenbach, G. Le Saout, D. Kulik, K. Scrivener. *Cem. Concr. Res.* 75 (2015) 91–103.
[24] P. Rejmak, J.S. Dolado, M.J. Scott, A. Ayuela. *J. Phys. Chem. C.* 116 (2012) 9755–61.
[25] E. Bernard, B. Lothenbach, D. Rentsch, I. Pochard, A. Dauzères. *Phys. Chem. Earth.* 99 (2017) 142–57.
[26] D. Nied, K. Enemark-Rasmussen, E. L’Hôpital, J. Skibsted, B. Lothenbach. *Cem. Concr. Res.* 79 (2015) 323–32.
[27] E. Kapeluszna, Ł. Kotwica, A. Różycka, Ł. Gołek. *Constr. Build. Mater.* 155 (2017) 643–53.